New Reduced-Order Lithium-Ion Battery Model to Account for the Local Fluctuations in the Porous Electrodes

Igor Traskunov and Arnulf Latz*

Numerical simulations of microscopic transport processes in porous electrodes of lithium-ion batteries demonstrate the presence of spatially localized fluctuations of physical quantities on the microstructure scale. They can influence the macroscopic battery characteristics (for example, the degradation rates). These fluctuations cannot be captured in a straightforward manner by the widely used porous electrode theory by Doyle, Fuller, and Newman (DFN model). The latter treats the porous electrodes as macroscopically homogeneous composite materials; it reduces the computational costs of numerical simulations. Herein, a modification of the DFN model that incorporates the local fluctuations but preserves the computational efficiency is proposed. Numerical simulation examples are presented that test the accuracy of the reproduction of the local fluctuations. The main new feature lies in the mathematical representation of the slow transport processes in the active material and their influence on the macroscopic reaction rates. The model is rooted in the rigorous mathematical analysis of the transition from a microscopic, microstructure-resolving transport and reaction description to a macroscopic, volume averaging-based one. The model construction methodology is open for further modifications for the applications in which some of the assumptions should be dropped, or description of new processes, reactions, phases, etc. should be incorporated.

I. Traskunov, Prof. A. Latz
Electrochemical Multiphysics Modeling
Helmholtz Institute Ulm for Electrochemical Energy Storage (HIU)
Helmholtzstraße 11, Ulm 89081, Germany
E-mail: igor.traskunov@dlr.de

I. Traskunov, Prof. A. Latz
Institute of Engineering Thermodynamics
German Aerospace Center (DLR)
Pfaffenwaldring 38-40, Stuttgart 70569, Germany

I. Traskunov, Prof. A. Latz
Faculty of Natural Sciences
University of Ulm
Ulm 89069, Germany

The ORCID identification number(s) for the author(s) of this article can be found under https://doi.org/10.1002/ente.202000861.

1. Introduction

The lithium-ion battery (LIB) is an important electrochemical energy storage technology. Various theoretical models have been developed to characterize them, from the atomistic level to the electrotechnical one, aiming at the prediction of a wide range of properties, from the elementary reaction potentials to the aging rates over many cycles. Naturally, these models build up a hierarchy of length and time scales, each level dealing only with the scale-relevant information.[1,2]

Porous medium is an important component of the battery electrodes and of the other chemical systems. Its presence introduces an additional scale separation between the processes inside the pores and the dynamics of the electrodes as a whole. The models suitable for the former are based on the continuous medium dynamics representation of the transport phenomena and of the reactions; mathematically, it is a set of partial differential equations (PDEs) with boundary conditions. We will use the term "microscopic" for these models. On the level of the electrode as a whole, it can be treated as a homogeneous composite material; here, the theoretical models are needed that describe the transport and the reactions there on average, neglecting the fine details of the porous microstructure. We call these models and the scale "macroscopic." Due to the omission of the microscopic details, they are computationally more efficient than the microscopic models. A class of models that have been widely used in electrochemical engineering is originated by Doyle, Fuller, and Newman (DFN model).[3–6] Its basic ideas are rooted in the porous electrode theory by Newman and Tiedemann.[7] Over the years, the initial model was supplemented by the features describing multiple battery phenomena as, e.g., heat generation, mechanical deformation, degradation reactions, and phase transitions.[8–15]

An accurate theoretical description of LIBs based on scale-hierarchical models requires a rigorous definition of the rules according to which the upscaled parameters are obtained from the low-level solutions. In the derivation of DFN-type models, one usually utilizes a formal mathematical volume averaging procedure, whose examples for different electrochemistry modeling-relevant PDEs can be found in the previous studies.[2,16–19] The proper convergence of the quantities of interest to the ones in the resulting volume-averaged PDEs is, however, not always

**ADVANCED
SCIENCE NEWS**
www.advancedsciencenews.com

Energy Technology
Generation, Conversion, Storage, Distribution
www.entechnol.de

self-evident. To bridge this gap, a homogenization theory has been applied to the transition from the microscopic LIB models to the macroscopic ones, explaining how the solutions of the former's equations converge in some sense to the solution of the volume-averaged equations.[20–22] It has been indicated, by the means of numerical analysis, that homogenization cannot be fully applied to LIBs. Physically, it is due to the fact that the mass transport in the solid phase active material is usually very slow. To properly account for the effects arising from the active material transport, DFN models substitute the complex microstructure-induced diffusion patterns with the ones in primitive geometrical domains, such as a sphere. It serves the goals of maintaining computational efficiency and intuitive understanding well, but, to the best of our knowledge, no rigorous mathematical explanation of the spherical particle approximation has been given. This ambiguity can potentially affect the internal consistency of the hierarchical modeling approach to LIBs.

Indication of possible inconsistencies has been detected using numerical simulation tools, and the microstructure models either obtained with tomographic imaging techniques or generated artificially. It has been demonstrated that some local physical quantities inside the electrodes may exhibit a complex spatial variability.[2,23,24] In the previous study,[2] one of the objectives was precisely the comparison of a non-equilibrium thermodynamics-based microscopic LIB model with its macroscopic DFN counterpart. The authors demonstrated that, in the microscopic model-based numerical simulations, spatially localized fluctuations of the overpotential in the electrodes are clearly present, and, consistent with the volume averaging idea, DFN predictions hold on average. One might note that the fluctuations of this kind cannot be derived in a straightforward manner in the DFN framework; here, physical quantities are either volume-averaged or ascribed to the positions inside the effective spherical active material particle. For the quantities in the latter, spherical symmetry holds; overpotential is a surface-related variable and, therefore, is constant because of this symmetry. To incorporate the spatially localized overpotential fluctuations into the macroscopic description, one has to add new conceptual features outside of DFN. From the application point of view, the correct prediction of the range of overpotential or surface concentrations of lithium distributed over the surface of the particle will be crucial for capturing the probability of degradation phenomena. DFN calculates one single value for the overpotential at the point of the spherical representative particle on macroscopic scale. If this value is above or below a certain electrochemical potential, where side reactions are initiated, they will not be predicted by DFN but can be captured by the microscopic transport theory, which predicts a range of overpotentials being distributed across the surface of a non-spherical representative particle. Also, the degree of mechanical stress will depend on the predicted distribution of concentrations across the surface of the particle, which is not captured by the single concentration value of DFN. Therefore, the accurate microscopic model is able to capture the finite probability of side reactions as, e.g., plating and electrolyte degradation or mechanical deformations, where DFN may completely miss them. If strongly localized phenomena as side reactions cannot be accurately described on the macroscopic scale, non-negligible deviations between the microscopic and the macroscopic cell models predictions

arise as a consequence of the inconsistencies in internal upscaling rules.

In this article, we present a modification of DFN that captures precisely the local fluctuations in sense of the previous study.[2] In the light of the fact that the fluctuations are seen in the microstructure-resolving calculations, there may be a connection between the origins of this local variability and the general problem of the accurate transition between the microscopic and the volume averaging-based macroscopic models. Building on this insight, we use the results of our mathematical analysis of this transition, whose technical details will be published separately. We stress the mathematical rigorousness of our approach, and all the necessary approximations are mentioned explicitly, making it possible to later modify the model for the applications in which the approximations do not hold. One of the cornerstones of the derivation is the use of the Galerkin method to obtain a reduced-order representation of the lithium diffusion equation. One may say that this representation substitutes the spherical particle primitives of the porous electrode theory as a way to compress the model-relevant microstructure information. The particular robustness of this compression is due to the prior knowledge of the solution properties that can be extracted using our mathematical framework. The resulting model's computational efficiency is on par with that of DFN. Special attention is given to the reproducibility of the local fluctuation characteristics.

The structure of this article is as follows. In Section 2, we start with reviewing the microscopic cell model and the corresponding DFN version relevant for the reaming article's text. Some methodological comments about wider families of models and the use of our approach beyond this article's narrow topic are presented. Then, we provide a summary covering the topic of the electrode localized fluctuations, their origin, and possible role, in Section 3. An argument in support of the association between them and the particle anisotropy (first of all, the shape anisotropy) is given. In Section 4, we review the mathematical analysis of the transition between the microscopic cell models and the volume averaging-based models, which imposes limitations on the possible models that accurately capture the homogenization limit solutions. Finally, in Section 5, we sum up the derivation of the new reduced-order model using the Galerkin method and compare it with the DFN model. The details of the new model's numerical implementation for realistic active material particles are outlined, and the accuracy is tested.

2. The Microscopic and DFN Models of LIBs

In this section, we will review, for the feature references, two main LIB models related to the subject of this article: the microscopic model by Latz and Zausch[2] and a basic DFN model. A class of models is generally referred to as the porous electrode theory, DFN or P2D models, which may include description of various cell phenomena besides the main cell reaction. To be more specific, we outline here the porous electrode theory-based model used in the previous study[2] as a macroscopic counterpart to the microscopic model from this article. From the electrochemistry perspective, these pair of models cover only the intercalation of lithium in electrodes. A few remarks will be

ADVANCED
SCIENCE NEWS
www.advancedsciencenews.com

Energy Technology
Generation, Conversion, Storage, Distribution

www.entechnol.de

made at the end of this section regarding the applicability of this article's methodology to the LIB models that include side reactions, etc.

In the basic microscopic model, two types of phases are present: electrolyte and electrode active material (in the cathode and in the anode), that are represented by the corresponding geometric domains. Four fields define the cell state: lithium ion concentration c_e and electrochemical potential ϕ_e in electrolyte, and lithium ion concentration c_s and electrical potential Φ_s in the electrode active material. The fields are defined in the respective domains and obey PDEs. Concentrations of other components relevant for the electrochemistry (such as anions, neutral solvent molecules, and electrons) are calculated algebraically through the constraints imposed on the cell: mechanical equilibrium on the relevant time and space scales (constant pressure for the liquid electrolyte) and charge neutrality on the relevant time and space scales (the double layers are assumed to be infinitesimally small). The four equations for the four variables are

$$\frac{\partial c_e}{\partial t} = -\vec{\nabla} \vec{N}_e \tag{1}$$

$$\frac{\partial c_s}{\partial t} = -\vec{\nabla} \vec{N}_s \tag{2}$$

$$0 = -\vec{\nabla} \vec{j}_e \tag{3}$$

$$0 = -\vec{\nabla} \vec{j}_s \tag{4}$$

$\vec{N}_{e,s}$ is the lithium ion fluxes, and $\vec{j}_{e,s}$ is the electric current densities. The first two equations are the ion mass transport equations, and the remaining ones are the dynamic forms of the charge neutrality conditions. The model stipulates the following dependence of the currents and of the fluxes on the system state fields

$$\vec{j}_e = -\kappa_e \vec{\nabla} \phi_e - \kappa_e \frac{1-t_+}{F} \frac{\partial \mu_e}{\partial c_e} \vec{\nabla} c_e \tag{5}$$

$$\vec{j}_s = -\sigma_s \vec{\nabla} \Phi_s \tag{6}$$

$$\vec{N}_e = -D_e \vec{\nabla} c_e + \frac{t_+}{F} \vec{j}_e \tag{7}$$

$$\vec{N}_s = -D_s \vec{\nabla} c_s \tag{8}$$

where κ_e is the electrical conductivity of the electrolyte, σ_s is the electrical conductivity of the active material, $D_{e,s}$ denotes the lithium ion diffusion coefficient in the respective phase, t_+ is the lithium ion electrolyte transference number, and μ_e is the lithium ion chemical potential in the electrolyte.

As the fields and the corresponding equations are defined in different domains, four boundary conditions should be added on the boundaries between the domains to make the PDE problem closed. These conditions are

$$\vec{j}_s \cdot \vec{n}_{se} = i_0 \tag{9}$$

$$\vec{j}_e \cdot \vec{n}_{se} = i_0 \tag{10}$$

$$\vec{N}_s \cdot \vec{n}_{se} = \frac{i_0}{F} \tag{11}$$

$$\vec{N}_e \cdot \vec{n}_{se} = \frac{i_0}{F} \tag{12}$$

where $\vec{n}_{se}$ is the normal unit vector on the boundary, and i_0 is the local density of the faradaic current corresponding to the lithium oxidation/reduction in (de-)intercalation. i_0 is defined by the reaction kinetics and depends on the local c_e, ϕ_e, c_s, and Φ_s. We generally assume the Butler–Volmer kinetics of the type used in the previous study[2]

$$i_0 = 2i_{00}\sqrt{c_e c_s (c_s^{max} - c_s)} \sinh\left(\frac{F}{2RT}\eta\right) \tag{13}$$

but the applicability of the article's results is not restricted only to this functional form, except for the cases where we explicitly mention it. The reaction overpotential η can be calculated through the potentials on the interface and the open circuit potential (OCV) U_0 according to the formula

$$\eta = \Phi_s - U_0(c_s) - \phi_e \tag{14}$$

when one measures the chemical potential of lithium ions in the electrolyte relative to the metallic lithium.

For the mathematical completeness of the problem, additional boundary conditions are needed to specify the cell interaction with its environment, for example, the ones between the domains and the current collector. They can include the conditions specifying the charging protocols of the cells, such as CC (constant current), CV (constant voltage), or more complex ones. These conditions are not important for the understanding of the paper material, and we do not write them down here. The main features of the model important for the article's topic are graphically summarized in **Figure 1**A.

Let us turn our attention to the DFN model. Here, the electrode is treated as a microscopically homogeneous composite material, and its phases are not distinguishable. Mathematically, it means it is represented by a single domain. The cell state is described by the volume-averaged fields $c_e^{(av)}$, $\phi_e^{(av)}$, and $\Phi_s^{(av)}$ defined on this domain on which PDEs are solved. The active material is represented by an effective spherical particle whose radius R is chosen to fit the specific surface area and the porosity of the electrode. Because of this, ion concentration in the active material $c_s(r, \vec{x})$ is a function of distance to the sphere center r and of the location in macroscopic electrode domain $\vec{x}$.

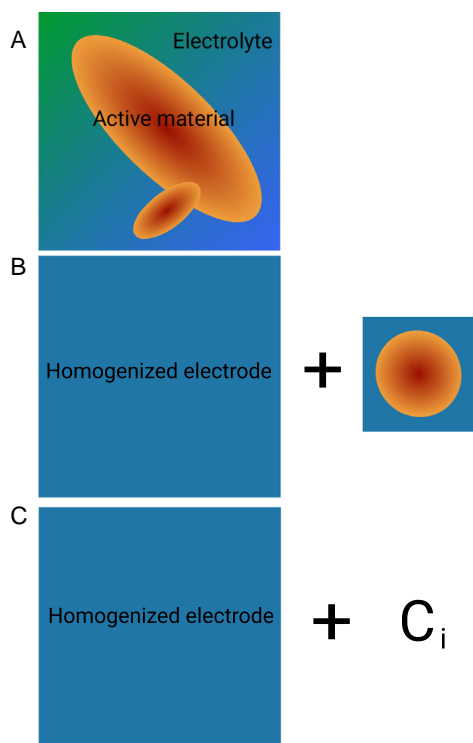The microscopic model Equation (1), (3), and (4) correspond to DFN equations

$$\frac{\partial c_e^{(av)}}{\partial t} = -\vec{\nabla} \vec{N}_e^{(av)} + \frac{1}{F} a i_0 \tag{15}$$

$$0 = -\vec{\nabla} \vec{j}_e^{(av)} + a i_0 \tag{16}$$

$$0 = -\vec{\nabla} \vec{j}_s^{(av)} - a i_0 \tag{17}$$

with constitutive relations (5)–(7) transforming into the ones for the spatially averaged fluxes and current densities

$$\vec{j}_e^{(av)} = -\kappa_e^{(eff)} \vec{\nabla} \phi_e^{(av)} - \kappa_e^{(eff)} \frac{1-t_+}{F} \frac{\partial \mu_e}{\partial c_e^{(av)}} \vec{\nabla} c_e^{(av)} \tag{18}$$

2000861 (3 of 13)

Figure 1. Graphical representation of the cell models from the article's text, with the main features. A) The microscopic model, with domains representing electrolyte and active material. B) DFN model, with a domain representing homogeneous upscaled electrode and a spherical particle domain for active material diffusion calculation. C) The reduced-order model, with a domain representing homogeneous upscaled electrode and the set of variables c_i, a compressed representation of lithium distribution in active material.

$$\vec{j}_s^{(av)} = -\sigma_s^{(eff)} \vec{\nabla} \Phi_s^{(av)} \tag{19}$$

$$\vec{N}_e^{(av)} = -D_e^{(eff)} \vec{\nabla} c_e^{(av)} + \frac{t_+}{F} \vec{j}_e^{(av)} \tag{20}$$

Transport coefficients $D_e^{(eff)}$ and $\kappa_e^{(eff)}$ are the effective composite material parameters and reflect the interaction between the transport phenomena and the microstructure morphology, and a is the specific interface area. Equation (2) and (8) preserve their form but for spherically symmetrical solutions, with the corresponding boundary condition

$$\frac{\partial c_s}{\partial t} = \frac{D_s}{r^2} \frac{\partial}{\partial r} \left(r^2 \frac{\partial c_s}{\partial r} \right)$$
$$D_s \frac{\partial c_s}{\partial r} \bigg|_{r=0} = 0 \tag{21}$$

The boundary condition on the sphere interface is the DFN equivalent of Equation (11)

$$D_s \frac{\partial c_s}{\partial r} \bigg|_{r=R} = -\frac{i_0}{F} \tag{22}$$

Due to the DFN treatment of the electrode as a single homogenized domain, the other interphase boundary conditions from

the microscopic theory are not needed. The matter and the charge exchange between the electrolyte and the active material are described instead by the source terms in Equation (18)–(20). The faradaic current density i_0 is assumed to depend on $c_e^{(av)}$, $\phi_e^{(av)}$, $\Phi_s^{(av)}$, and c_s the same way it depends c_e, ϕ_e, Φ_s, and c_s in the microscopic model. As with the microscopic counterpart, additional boundary conditions are needed to make the model mathematically closed, which represent the interaction of the electrodes with the current collectors and with their environment in general. They are not important for the article's topic and are omitted here. The graphical summary of the DFN model is given in Figure 1B.

As was mentioned at the beginning of the section, the basic microscopic model is quite simple in terms of the number of reactions and processes included, and one can, in principle, consider more sophisticated models by including side reactions, new phases, etc. They can be upscaled to the corresponding DFN-type models. In general, an algorithm for such upscaling can be summarized in the following steps: 1) the transport in the electrolyte on the microstructure scale is considered to be fast enough to justify its homogenized description; 2) the same is done to the electrical conduction in all the phases; 3) the reaction rates are homogenized as well; and 4) the ion mass transport in the solid active material microstructure is substituted by the mass transport in the representative spherical particle. Point 4) is critical because the ion diffusion in the electrodes is usually one of the slowest processes and a rate-limiting one. Its homogenization would introduce big errors that would keep the models from giving right predictions. We stress in this article that this step is critical for the mathematical consistency of the hierarchical modeling of LIBs. In the following, in this article's new macroscopic model, we will propose to substitute step 4 with a different approach. The assumptions behind steps 1–3 will still be assumed to hold.

Keeping this in mind, we can state that the model we will propose can be an alternative not only to the particular form of DFN and of the microstructure-resolving model we wrote down here but for a class of cell models that include a description of the side reactions, chemistry-mechanics coupling, reactions with additional chemical species, etc. One has to ensure, however, that steps 1 and 2 are valid. In step 3, the correctness of the reaction description with only the volume-averaged rate should be ensured only for the main lithium intercalation reaction. As for the side reactions, the possibility of the strong dependence of the rates on the local conditions prohibiting the use of simple averaged expressions in homogenized models is, in fact, the area where a new model extending DFN can be very instrumental for the battery research, as we emphasized in Section 1.

3. Local Fluctuations in Porous Electrodes

In this section, we summarize the important facts about the local fluctuations in the porous electrodes that motivated the DFN modification proposed in this article.

Latz and Zausch[2] investigated the cell thermal behavior predictions calculated with their microscopic cell model and with the corresponding volume-averaging model. The comparison of these models and the details that cannot be properly captured

**ADVANCED
SCIENCE NEWS**
www.advancedsciencenews.com

Energy Technology
Generation, Conversion, Storage, Distribution
www.entechnol.de

by the volume-averaging procedure were in the focus, such as, for example, the local hot spots. The microscopic model is a slightly modified version of the one from Section 2, with additional terms that represent the non-equilibrium thermodynamics-based coupling of the transport phenomena with temperature gradients. However, the inclusion of these gradients influenced the numerical predictions presented in the previous study[2] very weakly due to the negligible temperature variation on the cell scale, and the results relevant for this article are, thus, true for the basic isothermal model of Equation (1)–(8) as well.

In that study, considerable spatial fluctuations of the overpotential up to the order of 50 mV were observed in the microscopic model-based simulations. At the same time, the running average agrees remarkably well with the overpotential profile from the counterpart DFN-based simulation (Figure 7 in the previous study[2]). The presence of such fluctuations (and, potentially, of similar fluctuations of other physical quantities in the cell) may have important consequences in the battery modeling. Whenever there is a process whose dynamics is strongly influenced by the local conditions on the microstructure scale, making an accurate theory-based prediction about the rate of this process on the macroscopic scale becomes a nontrivial task requiring knowledge about the local fluctuation distribution, especially when the dependence on the local conditions is strongly sharp and non-linear. Examples of such processes may include side reactions (such as SEI growth or lithium plating), mechanical deformations of the particles, etc. They may contribute to the battery aging, and thus, their accurate analysis is important for the field.

At the same time, note that the standard DFN model based on Equation (15)–(22) cannot reproduce the desired local overpotential fluctuations. Indeed, the overpotential is an interface-related quantity; any solution of the problem (21) and (22) is spherically symmetric by construction; consequently, the overpotential is the same on the whole representative particle surface. The only spatial dependence appears on the volume-averaged scale. The spatial variation in the previous study,[2] contrary to this, happens on the microstructure scale. To capture it as computationally efficiently as calculation with DFN would do, a modification of the model is, therefore, needed.

Before we proceed to describe a candidate for such modification, we provide a qualitative explanation of the local overpotential fluctuations on an active material particle interface that will make the understanding of the mathematical arguments easier as follows. Let us consider the charging of one particle inserted into a homogeneous electrolyte with constant electrical potential. The electrolyte homogeneity may be due to high ion diffusivity and electrical conductivity, and the exact mechanism is not important here. We also assume that one can arbitrarily change the potential difference between the particle and the electrolyte, to control the faradaic reaction rate. The exact mechanism is not important here as well, as long as it preserves the homogeneity of the electrolyte and of the electrical potential. Under such conditions, if one has a constant lithium stoichiometry when the charging starts, the faradaic current i_0 is the same along the interface. If one neglects the lithium diffusion exchange between the different regions near the surface for a while, the rate of change of the average lithium concentration in one such region (denoted by index a) can be written down as

$$\frac{\partial \bar{c}_a}{\partial t} = \frac{S_a}{V_a} i_0 \qquad (23)$$

where V_a is the region's volume, and S_a is the surface area of the interface between the region and the electrolyte. When the particle is not spherical, the regions near the surface with different local curvature likely have different local ratios S_a/V_a, and a concentration difference between them will, thus, begin to emerge. The local OCV will change, and, according to formula (13), the overpotential will change too. Importantly, a difference between the values of these two quantities in the different regions will appear. This will, in turn, induce the local differences in i_0 affecting the rate $\partial \bar{c}_a/\partial t$. Finally, the diffusion will start to smooth out the concentration difference. These three factors (surface curvature variation, the lithium concentration feedback on i_0, and the diffusion) drive the amplitude of the concentration variation on the interface in different directions until they reach a dynamics equilibrium.

Importantly, this mechanism can explain the buildup of the differences between different locations on the interface of such physical quantities as OCV and overpotential. The fluctuations of the latter were visible in the numerical simulations in the previous study.[2] Note that for such effect to occur, only the non-spherical shape of a single particle is sufficient, and no other microstructure complexities are needed.

4. Mathematical Theory of the Local Fluctuations

To provide a more accurate estimate of the role of the particle shape factor we introduced earlier, we have developed a mathematical framework. It will help go beyond the purely qualitative analysis and answer a number of questions. First, if the local interfacial fluctuations due to the particle shape are big enough to explain the results in the previous study.[2] Second, how the strong spatial localization of the fluctuations allows for the applicability of DFN model, which is based on volume averaging and whose predictions have been generally proved to be correct. The answers to these questions will shed light on the foundations of the reduced-order model we are going to introduce.

Our method is rooted in the accurate analysis of the volume averaging procedure in lithium-ion cell models. The homogenization theory is usually used to derive the equations of DFN model (such as Equation (15)–(17)) from the microscopic transport-reaction laws (such as Equation (1)–(4)).[20–22] The homogenization theory is a formal mathematical ansatz that demonstrates how PDE problems can be upscaled when there is a length- and/or timescale separation and how the convergence of the upscaled problem solutions can be proved. Its applicability to the macroscopic LIB models construction has some limitations: it cannot be applied to the mass transport in the active material (thus justifying the introduction of the representative spherical particle in DFN). It was shown in the previous study[22] with numerical experiments; only a numerical model that includes the homogenization for some equations and the exact microscopic PDE problem for the slow mass transport gives the solution to which the exact solution converges in the scale separation limit. For our framework, we went beyond the standard homogenization assumptions and introduced additional

conditions on the system, to get more analytical results. We have used the homogenization together with other perturbation techniques. The mathematical details and the numerical tests will be published separately; here, we will present the physical motivations and the main results of our theory.

We started the analysis with listing all the small parameters that are related to the homogenization. The first

$$\delta_1 = \frac{L}{L_0} \tag{24}$$

is the ratio of the microstructure length scale L (for example, the active material particle size) to the macroscopic length scale L_0. The latter is not the electrode thickness, but rather the length scale on which the composition and the potentials in the electrode vary significantly to affect the intercalation reaction rate. As such, L_0 is related to the volume-averaged gradients in the electrode and depends on the cell operation conditions, such as C-rate, and not only on the electrode geometry. One can demonstrate that, with the physically realistic transport parameters of the cells, δ_1 almost always remains small. The second small parameter is the ratio of the microscopic time scale to the macroscopic one

$$\delta_2 = \frac{\tau_{\text{micro}}}{\tau_{\text{macro}}} \tag{25}$$

The definition of the time scales depends, again, on the whole operation regime of the cell. It can be shown that it scales with the averaged faradaic current density $\overline{i_0}$ such as

$$\delta_2 \sim \frac{|\overline{i_0}|}{i_{\text{cr}}} \tag{26}$$

where i_{cr} is the critical current density above which the transport limitations block charge or discharge of the active material particle. The situations in which the current is relatively close to i_{cr} are realistic, for example, in the fast charging protocols. Therefore, assuming δ_2 to be small may be not correct. From the formal mathematical point of view, it is exactly the condition that prevents the homogenization ansatz from being fully applicable to LIBs. Physically, it means that the active material lithium transport is slow and rate-limiting.

For our extensions of the standard DFN, two additional approximations should be introduced. The first one can be associated with the parameter

$$\delta_3 = \frac{S_{\text{interparticle}}}{S} \tag{27}$$

being small, where S is the particle surface area, and $S_{\text{interparticle}}$ is the interparticle contact area at which a direct lithium exchange between the particles not mediated by the electrolyte is possible. The condition $\delta_3 \ll 1$ is a mathematical expression of the fact that the microstructure can be reasonably good split into separate particles.

The smallness of δ_1 and δ_3 allows to expand the solution of the microscopic model into perturbation series

$$\begin{aligned}
\phi_e &= \phi_e^{(0)} + \phi_e^{(1)} + \ldots \\
c_e &= c_e^{(0)} + c_e^{(1)} + \ldots \\
\Phi_s &= \Phi_s^{(0)} + \Phi_s^{(1)} + \ldots \\
c_s &= c_s^{(0)} + c_s^{(1)} + \ldots
\end{aligned} \tag{28}$$

where the quantities with index 0 correspond to the zeroth-order terms, the quantities with index 1 are linear with respect to δ_1 and δ_3, and so on. Following our remarks mentioned earlier, we stress that the zeroth-order terms are not the solutions of the fully homogenized version of the microscopic cell model, but rather of a partially homogenized one. Namely, $\phi_e^{(0)}$, $\Phi_s^{(0)}$, and $c_e^{(0)}$ are the solution of the equations looking formally as Equation (15)–(17) but with different source terms. Because of the smallness of δ_3, $c_s^{(0)}$ splits into the separate solutions of the diffusion equations for the independent particles. These equations are mathematically connected to each other only through the common boundary condition parameters $\phi_e^{(0)}$, $\Phi_s^{(0)}$, and $c_e^{(0)}$.

The latter representation of the solution is identical to the one in the thought experiment charging we used in the previous section to explain how the surface fluctuations can emerge in just one active material particle. Combining that explanation with our mathematical analysis, we come to the conclusion that, even in the justifiable semi-homogenization limit ($\delta_1, \delta_3 \rightarrow 0$), the cell microstructure can induce the localized fluctuations on the particle interface.

The second approximation outside of the traditional homogenization conditions we use in the analysis is the linear approximation for the intercalation reaction rate dependence on the lithium concentration in the active material

$$i_0 = i_0^{(0)} + \beta(c_s - \tilde{c}) \tag{29}$$

Mathematically, such linear rate function can be obtained by resolving the exact one (such as formula (13)) into its Taylor series and dropping all the terms after the linear one. The resulting PDE problem is

$$\begin{aligned}
\frac{\partial c_s}{\partial t} &= \vec{\nabla}(D_s \vec{\nabla} c_s) \\
D_s \frac{\partial c_s}{\partial n}\bigg|_{\partial G} &= -\frac{1}{F}\left(i_0^{(0)} + \beta(c_s - \tilde{c})\right)
\end{aligned} \tag{30}$$

$\tilde{c}$ is the reference concentration that can be chosen in multiple ways, to ensure that the overall reaction rate is predicted accurately. In the following, we will give an example of one such choice. It is worth noticing that the accuracy of the linearization can be associated with another smallness of another parameter and, through this, with the overall cell dynamics, similarly to δ_1 and δ_2. The PDE problem in form (30) allows one to proceed much further in theoretical estimation how big the fluctuations are than the general dynamic laws (2), (8), and (11) would. Also, it provides valuable insights into the local reaction-diffusion dynamics. When $i_0^{(0)}$ and β do not depend on time, the solution of Equation (30) converges to a stationary gradient profile after a transient relaxation period. Two important dimensionless parameters emerge

$$\gamma = \frac{|\bar{i}_0|}{i_{cr}} \tag{31}$$

$$\rho = \beta L / F D_s \tag{32}$$

They control the fluctuation scale in the stationary c_s profile, together with the particle's shape. In real life cell dynamics, the parameters of system (30) can change with time, and the same is true for γ and ρ. We, however, assume that the dynamic solution tends to be close and gravitates to the stationary one. It is possible to derive approximate formulas to estimate how big the variation of the concentration in the stationary profile is. Here, we will concentrate on the aspects of this dependence that are relevant for the topic of this article.

First, we concentrate on the important, physically feasible case $\rho \to 0$, in which the standard deviation of lithium concentration on the particle surface behaves like

$$\delta c_s|_S \equiv \left(\int \frac{\mathrm{d}S}{S} (c_s - \overline{c_s}|_S)^2 \right)^{1/2} \sim c_m \gamma$$
$$\overline{c_s}|_S \equiv \int \frac{\mathrm{d}S}{S} c_s \tag{33}$$

c_m is the maximum possible concentration of lithium in the active material, and the exact proportionality coefficient depends on the particle shape and, naturally, becomes small when the particle is chosen to be close to sphere in shape. Recalling the argument about the ratio of the reaction current to the critical current from the discussion about the parameter δ_2 above and the definition of γ, one can see that the variation of c_s is not generally bound to be small relative to c_m. Even if, after a certain amplitude of $\delta c_s|_S$, the linearization assumption in problem (30) stops being accurate, our analysis provides strong mathematical argument for the conjecture that the particle shape-induced local fluctuation in the electrodes is not negligible, thus answering one of the questions we posed at the beginning of this section.

The second important aspect of the behavior of the solution of problem (30) is its dependence on parameter ρ. It can be shown that, when $\rho \to \infty$, $\delta c_s|_S \to 0$; more precisely, $\delta c_s|_S \sim 1/\rho$. The numerical results presented in the following indicate that an inverse (although not necessary an inversely proportional) relation between $\delta c_s|_S$ and ρ holds for spheroid-like particle shapes inside a wide window of parameter ρ values, not only in the asymptotic case.

In the numerical section, we will also look at the dependence of $\delta c_s|_S$ on γ. It should be noted that, in the simulation of the cell with the parameters close to the realistic ones, it is hard to track the γ dependence separately from the ρ dependence in general. At first, looking at definition (31), one may expect the γ dependence to be identical to the current dependence. But, in reality, γ and ρ both dynamically depend on the current: ρ is effectively a slope of the reaction kinetics versus c_s; in the case of the Butler–Volmer formula (13), for example, it depends on the overpotential, which, in turn, is conditioned on the current. The above-mentioned case $\rho \to 0$ is the one in which the role of ρ can be neglected, and one can simply state that $\delta c_s|_S$ grows with $|\bar{i}_0|$. In the numerical simulation experiments, we will investigate exactly this case.

The answer to the second question from the beginning of this section, about the influence of our findings to the applicability of DFN models, can be stated as follows. The mathematical form and the physical meaning of the effective parameters of the volume-averaging equations of DFN (15)-(17) are accurate within physically reasonable assumptions ($\delta_1, \delta_3 \to 0$). The volume source terms, however, do not necessary evolve according to the DFN predictions. Our theory predicts only that, for arbitrary particle shapes, the discrepancy between the volume averaged sources in the DFN and the microscopic model should generally grow with parameter γ, which is not generally small. Interestingly, the results in the previous study[2] and the numerical simulations presented in the following in this article indirectly support the conjecture about the closeness between the DFN source terms and the ones due to the exact solution, by demonstrating the good agreement among the volume-averaged overpotentials, OCV, surface lithium concentrations, and the corresponding DFN values.

5. Reduced-Order Model

5.1. Motivation for the Model Choice

To propose a DFN modification, we first make a list of the important requirements that the model in question should desirably meet, based on the analysis in the previous sections. 1) The method should preserve the homogenized equations of DFN for the processes for which the homogenization is accurate. 2) The active material lithium dynamics should be represented as the one of an ensemble of isolated active material particles interacting with the homogeneous electrolyte and electric potential. 3) The predicted volume-averaged faradaic current dynamics should be close to the ones obtained in the microscopic model calculations. 4) The lithium concentration profiles in the models should generally be close to the stationary solutions of PDE problem (30). 5) The model should predict the interfacial variations of the physical quantities of interest, at least in a statistical sense (such as the spatial standard deviations, other statistical moments, etc.). 6) The model should be comparable with DFN in terms of computational efficiency.

The effective spherical particle microstructure representation in DFN is exactly the component that reduces the computational intensity of modeling diffusion in more complex domains. One can treat it not as a physical object but as a mathematical abstraction, a reduced-order representation of the diffusion equation PDE problem that captures some basic characteristics of the solution at the expense of the others. We can choose another such representation that meets the requirements listed earlier. A good candidate is the discrete approximation of PDEs obtained with the Galerkin method. The method is widely used in the numerical mathematics, in particular in finite-element method (FEM) applications. One can learn about the details in the FEM literature (for example, in the previous study[25]).

In essence, the Galerkin method substitutes a differential equation over the set of continuous functions with a system of equations over a finite set of variables. The functions themselves are approximated by superpositions of a number of basis functions. In this sense, Galerkin's ansatz is a problem order

ADVANCED
SCIENCE NEWS
www.advancedsciencenews.com

Energy Technology
Generation, Conversion, Storage, Distribution
www.entechnol.de

reduction. When one has a prior information about the solution, one can choose a small basis set that gives an accurate solution representation at a small computational cost.

As we know that what we need to reproduce well are the stationary solutions of problem (30), we can choose the basis functions that capture the c_s profiles in these solutions in typical active material particles. Important notes should be done here. In FEM applications of the Galerkin method, a set of basis functions (finite elements) is usually chosen that accurately reproduces the complete function with necessary numerical resolution, the elements being usually localized on the numerical grid cells. Contrary to this, we are satisfied with the set that only captures the necessary integral characteristics of the solution. A good set will be proposed and tested in the numerical section as follows.

An important argument for the method's choice is that, in principal, Galerkin's approach is supported by the mathematical theorems about the solution convergence and stability, the details to be found in the literature. It ensures that, if the solution's accuracy is not satisfactory, one can always fix it by adding additional basis functions. In our investigation of the transition from the microscopic cell models to the homogenization-based ones, we try to follow the rigorous derivation whenever it is possible, listing all the mathematical approximations we make, and the transition from the exact diffusion equation to Galerkin's equations is controlled by the known error estimates.

5.2. Particle Ion Transport Equations in the Reduced-Order Model

Here, we are going to outline the formal derivation of the model representation of PDE problem (30) using the Galerkin method, without giving the mathematical explanation of the steps. One has to rewrite the problem in the so-called weak formulation. First, the equation is multiplied by an arbitrary function $\psi(\vec{x})$, then integrated over the problem domain G (which in this context is the space occupied by one particle, not the electrode or the whole cell), and transformed using Gauss's divergence theorem

$$\int_G dx \psi \frac{\partial c_s}{\partial t} = -\int_G dx D_s \vec{\nabla} c_s \cdot \vec{\nabla} \psi + \int_{\partial G} \vec{d} S \psi D_s \vec{\nabla} c_s \tag{34}$$

Substituting the boundary condition from Equation (30) into Equation (34), one obtains the weak formulation

$$\int_G dx \psi \frac{\partial c_s}{\partial t} = -\int_G dx D_s (\vec{\nabla} c_s \cdot \vec{\nabla} \psi) - \int_{\partial G} dS \psi \frac{1}{F} \beta (c_s - \tilde{c})$$
$$- \int_{\partial G} dS \psi \frac{1}{F} i_0^{(0)} \tag{35}$$

At this point, to write down the final equations in the closed form, one has to specify the reference concentration $\tilde{c}$. We set it to be an average surface concentration

$$\tilde{c} = \int_{\partial G_r} \frac{dS}{S} c_s \tag{36}$$

S is the part of the particle surface area exposed to the faradaic reaction with the electrolyte, and the integration over ∂G_r means

the integration over this part of the interface. This choice will make it easy to analytically express the galvanostatic particle charge constraint in the numerical simulation section and will ensure an accurate total current representation, but it is not the only possible choice. Let us assume that, in this section, $i_0^{(0)}$ and β on the passive interface are equal to 0. Note that it means, some surface integrals in the following are equal when taken both over ∂G and over ∂G_r. In the next step, one has to choose a set of basis functions $\psi_i(\vec{x})$, $1 \leq i \leq n$. The representation of the lithium density as a linear combination of these functions $c_s = \sum_i c_i \psi_i$ is formally substituted into the weak formulation, with the arbitrary function $\psi(\vec{x})$ changing to one of ψ_i.

$$\sum_i \int_G dx \psi_j \psi_i \frac{\partial c_i}{\partial t} + \sum_i \int_G dx \psi_j \frac{\partial \psi_i}{\partial t} c_i$$
$$= -\sum_i \int_G dx D_s \left(\vec{\nabla} \psi_j \cdot \vec{\nabla} \psi_i \right) c_i -$$
$$- \frac{1}{F} \sum_i \left(\int_{\partial G} dS \psi_j \beta \psi_i - \int_{\partial G} dS \psi_j \beta \int_{\partial G_r} \frac{dS}{S} \psi_i \right) c_i$$
$$- \frac{1}{F} \int_{\partial G} dS \psi_j i_0^{(0)} \tag{37}$$

Let us introduce typical diffusivity $\tilde{D}_s$, typical length scale L, typical β as $\tilde{\beta}$, typical current density $\tilde{i}$, and particle volume V; a set of matrices

$$A_{ji} = \int_G \frac{dx}{V} \psi_j \psi_i \tag{38}$$

$$B_{ji} = \int_G \frac{dx}{V} \psi_j \frac{\partial \psi_i}{\partial t} \tag{39}$$

$$M_{ji} = \int_G \frac{dx}{V} \frac{D_s}{\tilde{D}_s} L^2 (\vec{\nabla} \psi_j \cdot \vec{\nabla} \psi_i) \tag{40}$$

$$A_{ji}^{(S)} = \int_{\partial G} \frac{dS}{S} \frac{\beta}{\tilde{\beta}} \psi_j \psi_i - \int_{\partial G} \frac{dS}{S} \frac{\beta}{\tilde{\beta}} \psi_j \int_{\partial G_r} \frac{dS}{S} \psi_i \tag{41}$$

and a tuple

$$a_j^{(S)} = \int_{\partial G} \frac{dS}{S} \frac{\beta}{\tilde{\beta}} \psi_j \frac{i_0^{(0)}}{\tilde{i}} \tag{42}$$

With these notations, one can rewrite the set of Equation (37) as

$$\sum_i A_{ji} \frac{dc_i}{dt} = -\sum_i B_{ji} c_i - \frac{\tilde{D}_s}{L^2} \sum_i M_{ji} c_i - \frac{S\tilde{\beta}}{FV} \sum_i A_{ji}^{(S)} c_i - \frac{S\tilde{i}}{FV} a_j^{(S)} \tag{43}$$

There is a certain freedom in the choice of the basis functions. In general case, using functions explicitly depending on time ($\partial \psi_i / \partial t \neq 0$) may be beneficial to accurate representations of transient processes in the active material particles. Here, we neglect the time dependence of ψ_i; hence, everywhere $B_{ji} = 0$. The choice of ψ_i that helps build an accurate yet efficient cell model will be discussed in the numerical simulation section. In this theoretical section, we will demonstrate how imposing

certain restrictions on ψ_i allows rewriting Equation (43) in a form more suitable for understanding of the physical meaning of the terms and of the way the equations encode or compress the information about the local fluctuations. To this end, we chose the basis functions to be dimensionless, to make the matrices and the tuple dimensionless. Then, we fix the particle length scale according to the rule $L = V/S$ and the basis functions dependence on L

$$\psi_i(\vec{x}) \equiv \psi_i^{(0)}(\vec{x}/L) \tag{44}$$

where functions $\psi_i^{(0)}$ do not depend on L explicitly. After this, the following is true, when β and D_s are constant and equal to $\tilde{\beta}$ and $\tilde{D}_s$, respectively: quantities A_{ij}, M_{ji}, $A_{ji}^{(S)}$, and $a_j^{(S)}$ are defined only by the particle's shape. More precisely, they are either equal for the geometrically similar particles or can be made equal by the coordinate system axes rotation. In particular, they do not depend on L or on any physical parameters of the cell or of the charging process. As an example, for matrix A_{ij}, introducing new coordinates $\vec{x} = L\vec{y}$ and the particle volume in the new coordinate system $V^{(0)} = V/L^3$, one obtains

$$A_{ji} = \int_G \frac{dx}{V} \psi_j(\vec{x})\psi_i(\vec{x}) = \int_{G^{(0)}} \frac{d\gamma}{V^{(0)}} \psi_j^{(0)}(\vec{\gamma})\psi_i^{(0)}(\vec{\gamma}) \tag{45}$$

Domain $G^{(0)}$ occupied by the particle in the coordinate system $\vec{\gamma}$ is the same for all geometrically similar particles or can be made the same through rotation, hence the invariance of A_{ij}. In summary, one can say that the matrices and tuples (38)-(43) encode only the information about the particle's shape. When possible inhomogeneity of β and D_s is accounted for, they encode the microscopic electrode anisotropy in general. On the other hand, the coefficients in front of the matrices and the tuples in Equation (43) reflect the main physics of the active material particle interaction with the environment (electrochemistry kinetics, electric current, and diffusion). Using the notation of the previous section, setting $B_{ji} = 0$, one rewrites Equation (43) as

$$\sum_i A_{ji}\frac{dc_i}{dt} = -\frac{\tilde{D}_s}{(V/S)^2}\left(\sum_i M_{ji}c_i + \rho\sum_i A_{ji}^{(S)}c_i + c_m\gamma a_j^{(S)}\right) \tag{46}$$

The parameters γ and ρ from Section 4 enter the equations explicitly. In this formulation, different terms are clearly associated with the different driving forces mentioned earlier, whose equilibrium defines the stationary concentration gradient profile in the particle encoded in values c_i. The ρ value being big or small indicates which of these forces is dominant.

5.3. The Complete Set of Model Equations

In this section, we put together all the equations for the complete reduced-order cell model. We will compare them with two models presented in Section 2, especially with DFN. To avoid overgeneralization, to provide general understanding and to keep all the formulas compatible with the variant we used for the numerical simulations in the following, we look at the case when the kinetic law defining the dependence of faradaic reaction rate on potentials and concentrations $i_0(c_e, \phi_e, c_s, \Phi_s)$ does not

explicitly depend on the coordinates on the interface of a single particle. It is worth noting that such dependence can potentially be a part of the model and, in fact, is a valid source of the local surface fluctuations we aim to capture. In the Butler–Volmer kinetics (13), it would mean that i_{00} is different for different interface parts. Physically, such differences can be induced by different crystalline surfaces exposed to the electrolyte.

The model is structured as follows. As in DFN, the electrode is a microscopically homogeneous composite material and is represented by a single geometrical domain, and the volume-averaged fields $c_e^{(av)}(\vec{x})$, $\phi_e^{(av)}(\vec{x})$, and $\Phi_s^{(av)}(\vec{x})$ are defined on it. The active material lithium concentration is represented by a tuple of numbers $c_{ik}(\vec{x})$. Index i denotes different basis functions ψ_i, and index k denotes different types of particles (shape, material, etc.). When one resolves i_0 into the power series of c_s around $\tilde{c}$ defined according to Equation (36), to get the linearized kinetics of problem (30), the absence of the explicit coordinate dependence in $i_0(c_e, \phi_e, c_s, \Phi_s)$ means the absence of such dependence in $i_0^{(0)}(c_e, \phi_e, \tilde{c}, \Phi_s)$ and $\beta(c_e, \phi_e, \tilde{c}, \Phi_s)$ too.

Given these remarks, the equations of the type of Equation (43) for the variables c_{ik} in which the dependence on the other model variables and on the particle type k is shown explicitly are

$$\sum_i A_{jik}\frac{dc_{ik}}{dt} = -\frac{\tilde{D}_{sk}}{L_k^2}\sum_i M_{jik}c_{ik} - \frac{S_k\beta_k\left(c_e^{(av)}, \phi_e^{(av)}, \tilde{c}_k, \Phi_s^{(av)}\right)}{FV_k}$$
$$\times \sum_i A_{jik}^{(S)}c_{ik} - \frac{S_k i_{0k}^{(0)}\left(c_e^{(av)}, \phi_e^{(av)}, \tilde{c}_k, \Phi_s^{(av)}\right)}{FV_k}a_{jk}^{(S)} \tag{47}$$

$$\tilde{c}_k = \sum_i a_{ik}^{(S)}c_{ik} \tag{48}$$

The remaining equations of the cell model have the same form as the corresponding DFN equations, with the same physical meaning of the parameters, but with slightly different source terms

$$\frac{\partial c_e^{(av)}}{\partial t} = -\vec{\nabla}\vec{N}_e^{(av)} + \frac{1}{F}\sum_k a_k i_{0k}^{(0)}\left(c_e^{(av)}, \phi_e^{(av)}, \tilde{c}_k, \Phi_s^{(av)}\right) \tag{49}$$

$$0 = -\vec{\nabla}\vec{j}_e^{(av)} + \sum_k a_k i_{0k}^{(0)}\left(c_e^{(av)}, \phi_e^{(av)}, \tilde{c}_k, \Phi_s^{(av)}\right) \tag{50}$$

$$0 = -\vec{\nabla}\vec{j}_s^{(av)} - \sum_k a_k i_{0k}^{(0)}\left(c_e^{(av)}, \phi_e^{(av)}, \tilde{c}_k, \Phi_s^{(av)}\right) \tag{51}$$

Numbers a_k are the partial specific surface areas of the particle type k. The fluxes and the currents depend on the cell state according to formulas (18)-(20). Figure 1C gives a graphical representation of the reduced-order model. A comparison with Figure 1B emphasizes that the crucial differences with the traditional DFN are the active material diffusion representation and its mathematical binding to the remaining transport phenomena.

It is important to stress again that the presented model describes the same transport and chemical processes as the microscopic model and the DFN model there. More generally, by adding additional side reactions into every one of them, three

**ADVANCED
SCIENCE NEWS**
www.advancedsciencenews.com

Energy Technology
Generation, Conversion, Storage, Distribution
www.entechnol.de

families of models may be generated. For a model from DFN class to be applicable, the conditions outlined in Section 2 should be fulfilled. For the models of the family similar to the one presented in Equation (47)–(51), additionally, the conditions of the perturbation theory applicability from Section 4 should hold. The main advantage is the accurate account of the local interface fluctuations.

6. Implementation and Numerical Results

The objective of this section is to propose a minimal set of basis functions for the reduced-order method that reproduces the necessary characteristics of the local shape-induced concentration fluctuations and to assess the accuracy.

The proposed basis set $\{\psi_i\}$ consists of the polynomials up to power 2

$$\{1, x, y, z, x^2, xy, \ldots\} \tag{52}$$

ten functions in total. The following heuristic arguments can be provided in the support of this choice. When one considers a spherical particle, the stationary spherically symmetrical solution of problem (30) is

$$c_s \sim r^2 + \text{const} = x^2 + y^2 + z^2 + \text{const} \tag{53}$$

One can expect that when we gradually change the shape from spherical to slightly elongated, the parabolic function is still a good representation, but it becomes slightly squeezed. Also, from the perspective of angular dependence, a stationary solution with the polynomials up to power 2 with a properly chosen coordinate system contains only the spherical harmonics $Y_l^m(\theta, \phi)$ up to $l = 2$. It means, the basis captures only the solution anisotropy on big angles of the order $\pi/2$, not the small angular variations. It agrees with our goal to build an economical model capturing the averaged, coarse surface fluctuation characteristics, not the fine details. Borrowing the terminology from the theoretical electrodynamics, one can say that a choice of the basis functions including only the spherical harmonics with $l \leq 2$ reflects only the dipole and the quadrupole components of the angle-sensitive solution variation.

As the accuracy of the reduced-order model in capturing the local fluctuations is in the focus of this article, we chose an example for the numerical analysis, which allows to estimate this particular accuracy separately. Such system is a one-particle system, similar to the one we used in Section 3 argument. In the multiple-particle simulation, the precision of one-particle modeling would be hidden in the complexity. The active material and electrolyte material parameters are chosen that are close to the ones of the real cells. The particle shape is spheroid with an aspect ratio of 0.5 and the main axis 10^{-3} cm. The physical parameters are listed in **Table 1**, with the notations from the article's text. OCV as a state of charge (SOC) function is

Table 1. Physical parameters for the article's numerical simulation examples.

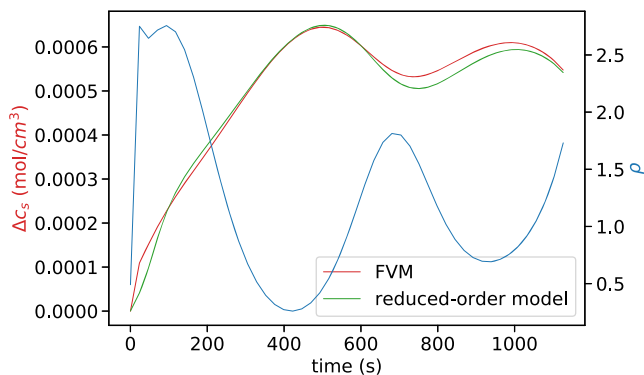| Parameters	Value	Units
$c_s^{(\text{initial})}$	2.639×10^{-3}	mol cm^{-3}
c_m	2.4681×10^{-2}	mol cm^{-3}
D_s	10^{-10}	$\text{cm}^2\,\text{s}^{-1}$
c_e	1.2×10^{-3}	mol cm^{-3}
i_{00}	0.002	$\text{A cm}^{-2.5}\,\text{mol}^{-1.5}$

$$\begin{aligned}
U_0(V) &= 0.6379 + 0.5416 \cdot \exp(-305.5309 \cdot \text{SOC}) + \\
&\quad + 0.044 \cdot \tanh(-(\text{SOC} - 0.1958)/0.1088) - \\
&\quad - 0.1978 \cdot \tanh((\text{SOC} - 1.0571)/0.0854) - \\
&\quad - 0.6875 \cdot \tanh((\text{SOC} + 0.0117)/0.0529) - \\
&\quad - 0.0175 \cdot \tanh((\text{SOC} - 0.5692)/0.0875)
\end{aligned} \tag{54}$$

The SOC definition is physical: $\text{SOC} = c_s/c_m$. The particle is subjected to the galvanostatic charge with average current density 10^{-4} A cm^{-2}. It roughly corresponds to C-rate 3C. We do not control voltage cutoffs explicitly and instead start the charge from initial homogeneous state $c_s = c_s^{(\text{initial})}$ and stop at an arbitrary time of 1200 s, when the local SOC on the surface is close to 100%. Note our comment mentioned earlier that some approximation errors tend to grow with current/C-rate; this observation ensures that, when our model is accurate for the high C-rates, it tends to be accurate for the low C-rates as well. In this section's simulations, we assume full homogenization ($\delta_1 = 0$), in line with Section 3 example. It means, variables c_e, ϕ_e, and Φ_s are constant on the particle scale, and Equation (43) is fully decoupled from the other equations.

The reference solution to which we compared the results of our reduced-order model is the finite volume method (FVM) implementation on a cubic mesh with 60 control volumes per main spheroid axis, with explicit time integration. The current version of the reduced-order model is an ordinary differential equation system with ten variables; its full charge simulation using an implementation in Python package Scipy takes less than 1 s and is, therefore, very robust computationally. The data from the simulation results have been analyzed. The time evolution of the standard deviation of two physical quantities on the surface is plotted: lithium concentration (**Figure 2**) and local OCV (**Figure 3**). The comparison with the same quantities in the reference solution is remarkable for such seemingly simple model.

Figure 2 additionally contains the dynamics of parameter ρ introduced in the mathematical theory of the fluctuations. We mentioned that there exists an inverse relation between the surface concentration variation and ρ, at least for big values of ρ. One can notice that in the plot, they almost always move in the opposite directions. It indicates that for the spheroid geometry, the inverse relation holds for finite values of ρ too: indeed, it varies between 0 and 3, which cannot be considered big.

Figure 4 and **5** demonstrate how the dynamics of the surface fluctuations changes when one changes the C-rate/current density. First, one notices that, with the decreasing C-rate, ρ becomes

**ADVANCED
SCIENCE NEWS**

www.advancedsciencenews.com

Energy Technology
Generation, Conversion, Storage, Distribution

www.entechnol.de

Figure 2. Time evolution of the lithium concentration standard deviation on the active material particle surface in FVM and in the reduced-order model numerical simulations for the 3C charge rate case. Simultaneous evolution of parameter ρ introduced in the mathematical theory is plotted.
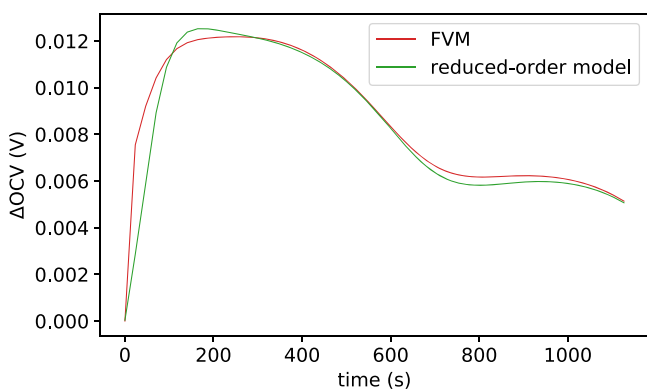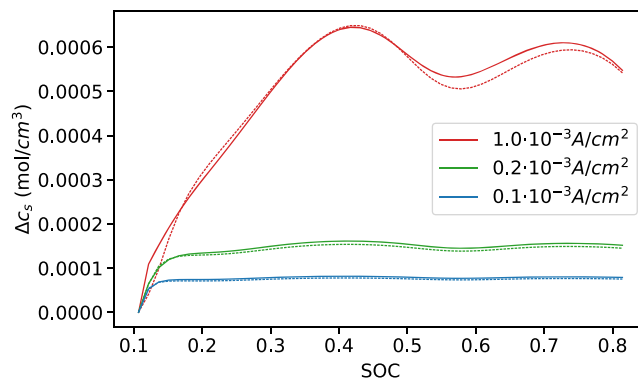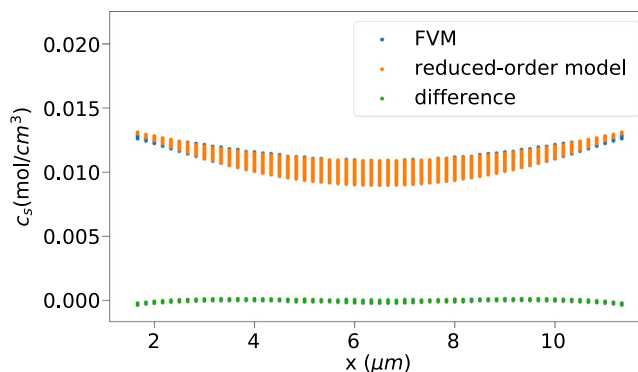

Figure 3. Time evolution of the OCV standard deviation on the active material particle surface in FVM and in the reduced-order model numerical simulations for the 3C charge rate case.
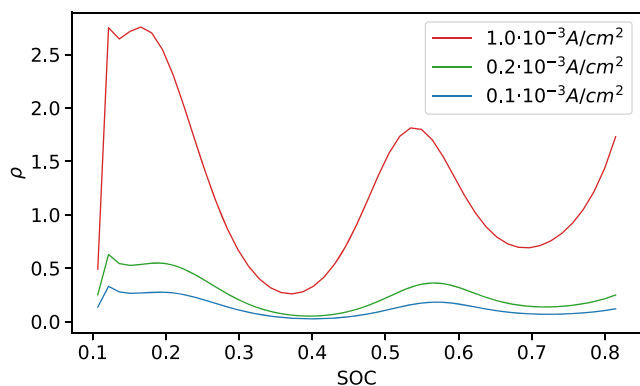
Figure 4. Comparison of the evaluation of parameter ρ introduced in the mathematical theory for different CC charge FVM simulations. The charge is characterized by the averaged current density through the particle surface. Here, SOC is the averaged surface SOC.

closer to zero. With this, we end up with the case $\rho \to 0$ presented in the introduction of the mathematical theory of the fluctuations. As we noticed there, in this case, the dependence of the


Figure 5. Comparison of the evaluation of lithium concentration standard deviation on the active material particle surface for different CC charge simulations. The charge is characterized by the averaged current density through the particle surface. Here, SOC is the averaged surface SOC. FVM simulation results are plotted with solid lines, and the reduced-order model results with dashed lines.
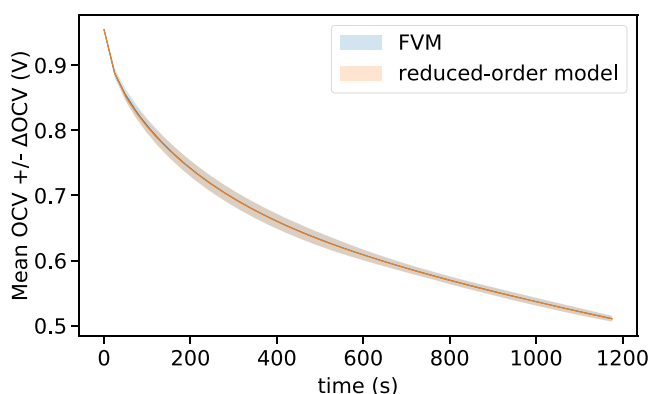

Figure 6. Snapshot of the lithium concentration in active material particle in FVM and in the reduced-order model numerical simulations at $t = 514.3$ s for the 3C charge rate case. The concentration profile is projected onto the axis X along the main axis of the spheroid particle.

surface concentration variation on current/C-rate/parameter γ is effectively dynamically decoupled from the dependence on ρ and is governed by estimate (33). Indeed, it is exactly what we see in Figure 5: first, the fluctuations decrease with decreasing current; second, after a short transient equilibration, they become almost constant in the smallest C-rate case, not sensitive to the peaks and valleys of the ρ dynamics. Note that, although the discrepancy between the FVM predictions and the ones of the reduced-order model grows with C-rate, the relative error stays roughly the same.

To emphasize the model accuracy not only on the integral quantities level, **Figure 6** gives a screenshot of the volume concentration distributions together with the point-by-point difference between the model and the FVM. We compared the fluctuation scale to their respective averages (**Figure 7** and **8**), to give a reader the understanding of the respective scales. Note that the discrepancy between the average values of the model and of the reference solution is far smaller than the fluctuation measures. It reminds the results of the previous study,[2] where the averaged overpotentials for the microscopic model and for DFN are much
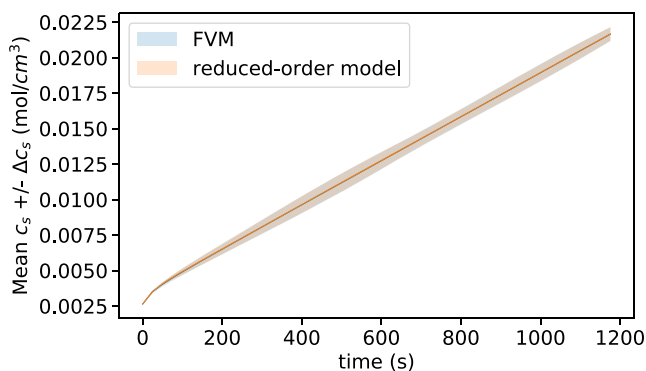
Figure 7. Time evolution of the lithium concentration mean and standard deviation on the active material particle surface in FVM and in the reduced-order model numerical simulations for the 3C charge rate case.

Figure 8. Time evolution of the OCV mean and standard deviation on the active material particle surface in FVM and in the reduced-order model numerical simulations for the 3C charge rate case.

closer to each other than the scale of their local fluctuations. At the moment, our theoretical analysis does not provide a general explanation for such property. It is, however, an interesting feature that replicates itself in two different numerical experiments, and an additional research may be needed.

7. Conclusion

This article introduces a new LIB model that is computationally effective and able to capture the microscopic spatial variation in the cell-relevant physical quantities on the microstructure level.

The model development was motivated by a number of investigations indicating the presence of such local fluctuations, their potential connection with the macroscopic cell characteristics, and their relation to the microstructure complexity.[2,23,24,26] We demonstrated that additions should be made to the widely used cell models based on porous electrode theory by Newman and co-workers (DFN models), to incorporate the effects due to these fluctuations. In proposing these additions, we strongly relied on the results of the mathematical analysis aimed at the classification of possible sources of the local fluctuations in the microstructure. As a byproduct of this

analysis, the limitations of the mathematical homogenization ansatz to the transport equations in the cells have been listed. As the homogenization of the equations plays an important role in the foundations of DFN equations, our analysis provides a theoretical filter for the assumptions that we make in the derivation.

The resulting model is as computationally robust as DFN. The numerical example is chosen, which emphasized the potential in the local fluctuation reproducibility. The Galerkin method is chosen as a main model order-reducing instrument, mainly due to its rigorous mathematical foundations and the available options to further improve the model's accuracy if needed.

Overall, the instruments and the approximations behind the model were chosen due to the combination of the mathematical analysis and of the heuristic solutions partially relevant to the particular lithium ion cell model in this article. Yet, the methodology can potentially be used to assist in accurate derivation of macroscopic models for more complex cell models, also for diffusion–reaction (electro-)chemistry systems in general. We emphasized the potential for such generalization in the article's text and related it to accurate tracking of the time and space scales of various chemical and physical processes.

Conflict of Interest

The authors declare no conflict of interest.

[1] A. A. Franco, *RSC Adv.* **2013**, *3* 13027.
[2] A. Latz, J. Zausch, *Beilstein J. Nanotechnol.* **2015**, *6* 987.
[3] M. Doyle, T. F. Fuller, J. Newman, *J. Electrochem. Soc.* **1993**, *140*, 1526.
[4] T. F. Fuller, M. Doyle, J. Newman, *J. Electrochem. Soc.* **1994**, *141* 1.
[5] M. Doyle, J. Newman, *Electrochim. Acta* **1995**, *40*, 2191.
[6] M. Doyle, J. Newman, A. S. Gozdz, C. N. Schmutz, J. M. Tarascon, *J. Electrochem. Soc.* **1996**, *143* 1890.
[7] J. Newman, W. Tiedemann, *AIChE J.* **1975**, *21*, 25.
[8] D. Bernardi, E. Pawlikowski, J. Newman, *J. Electrochem. Soc.* **1985**, *132* 5.
[9] C. R. Pals, J. Newman, *J. Electrochem. Soc.* **1995**, *142* 3274.
[10] C. R. Pals, J. Newman, *J. Electrochem. Soc.* **1995**, *142* 3282.
[11] W. B. Gu, C. Y. Wang, *J. Electrochem. Soc.* **2000**, *147* 2910.
[12] P. Arora, M. Doyle, R. E. White, *J. Electrochem. Soc.* **1999**, *146*, 3543.
[13] C. Monroe, J. Newman, *J. Electrochem. Soc.* **2003**, *150*, A1377.
[14] J. Christensen, J. Newman, *J. Electrochem. Soc.* **2006**, *153*, A1019.

[15] V. Srinivasan, J. Newman, *J. Electrochem. Soc.* **2004**, *151*, A1517.

[16] P. D. Vidtst, R. E. White, *J. Electrochem. Soc.* **1997**, *144*, 1343.

[17] C. Y. Wang, W. B. Gu, B. Y. Liaw, *J. Electrochem. Soc.* **1998**, *145* 3407.

[18] T. R. Ferguson, M. Z. Bazant, *J. Electrochem. Soc.* **2012**, *159*, A1967.

[19] M. Landstorfer, T. Jacob, *Chem. Soc. Rev.* **2013**, *42* 3234.

[20] W. Lai, F. Ciucci, *Electrochim. Acta* **2011**, *56*, 4369.

[21] F. Ciucci, W. Lai, *Transport Porous Media* **2011**, *88*, 249.

[22] V. Taralova, *Ph.D. Thesis,* **2015**.

[23] M. Ender, *J. Power Sources* **2015**, *282* 572.

[24] A. G. Kashkooli, E. Foreman, S. Farhad, D. U. Lee, K. Feng, G. Lui, V. De Andrade, Z. Chen, *J. Electrochem. Soc.* **2017**, *164*, A2861.

[25] G. Strang, G. Fix, *An Analysis of the Finite Element Method*, Wellesley-Cambridge Press, Wellesley, MA **2018**.

[26] R. Darling, J. Newman, *J. Electrochem. Soc.* **1997**, *144*, 4201.